Original Article

Development and validation of a CT-based radiomics nomogram for preoperative prediction of tumor histologic grade in gastric adenocarcinoma

Jia Huang[1,2*], Huasheng Yao[2,3*], Yexing Li[1,2], Mengyi Dong[2,4], Chu Han[2], Lan He[2], Xiaomei Huang[2,4], Ting Xia[2,5], Zongjian Yi[2,6], Huihui Wang[1,2], Yuan Zhang[2,4], Jian He[1,7], Changhong Liang[2], Zaiyi Liu[2]

[1]Graduate College, Shantou University Medical College, Shantou 515041, China; [2]Department of Radiology, Guangdong Provincial People's Hospital, Guangdong Academy of Medical Sciences, Guangzhou 510080, China; [3]School of Automation Science and Engineering, South China University of Technology, Guangzhou 510006, China; [4]Graduate College, Southern Medical University, Guangzhou 510515, China; [5]School of Medicine, South China University of Technology, Guangzhou 510006, China; [6]School of Biomedical Sciences and Engineering, South China University of Technology, Guangzhou 510006, China; [7]Department of Interventional Radiology, Cancer Center, Guangdong Provincial People's Hospital, Guangdong Academy of Medical Sciences, Guangzhou 510080, China

*These authors contributed equally to this work.

Correspondence to: Zaiyi Liu, PhD. Department of Radiology, Guangdong Provincial People's Hospital, Guangdong Academy of Medical Sciences, Guangzhou 510080, China. Email: liuzaiyi@gdph.org.cn.

Abstract

Objectives: To develop and validate a radiomics nomogram for preoperative prediction of tumor histologic grade in gastric adenocarcinoma (GA).

Methods: This retrospective study enrolled 592 patients with clinicopathologically confirmed GA (low-grade: n=154; high-grade: n=438) from January 2008 to March 2018 who were divided into training (n=450) and validation (n=142) sets according to the time of computed tomography (CT) examination. Radiomic features were extracted from the portal venous phase CT images. The Mann-Whitney U test and the least absolute shrinkage and selection operator (LASSO) regression model were used for feature selection, data dimension reduction and radiomics signature construction. Multivariable logistic regression analysis was applied to develop the prediction model. The radiomics signature and independent clinicopathologic risk factors were incorporated and presented as a radiomics nomogram. The performance of the nomogram was assessed with respect to its calibration and discrimination.

Results: A radiomics signature containing 12 selected features was significantly associated with the histologic grade of GA (P<0.001 for both training and validation sets). A nomogram including the radiomics signature and tumor location as predictors was developed. The model showed both good calibration and good discrimination, in which C-index in the training set, 0.752 [95% confidence interval (95% CI): 0.701−0.803]; C-index in the validation set, 0.793 (95% CI: 0.711−0.874).

Conclusions: This study developed a radiomics nomogram that incorporates tumor location and radiomics signatures, which can be useful in facilitating preoperative individualized prediction of histologic grade of GA.

Keywords: Adenocarcinoma; histologic grade; nomograms; stomach neoplasm; X-ray computed tomography

Submitted Sep 16, 2020. Accepted for publication Dec 22, 2020.
doi: 10.21147/j.issn.1000-9604.2021.01.08
View this article at: https://doi.org/10.21147/j.issn.1000-9604.2021.01.08

Introduction

Although the incidence of gastric cancer has decreased due to improved primary prevention, the mortality rate of gastric cancer still ranks third globally (1,2). In 2012, there were an estimated 952,000 new cases, of which nearly

three-quarters occurred in Asia, and more than two-fifths occurred in China (3). Gastric adenocarcinoma (GA) accounts for 95% of gastric malignancies (4). Referring to the World Health Organization (WHO) classification (5th edition), well and moderately differentiated GAs are classified as low-grade, and poorly differentiated GAs are classified as high-grade for better prognostic significance and reproducibility (5,6). The histologic grade of tumor differentiation has been proven to be associated with clinical outcomes (7-13). Patients with high-grade disease face a higher risk of lymph node metastasis and recurrence than those with low-grade disease, which leads to a poorer prognosis after curative surgery (14,15). Recent studies have demonstrated that patients with limited metastatic disease exhibit favorable overall survival after receiving neoadjuvant chemotherapy (16,17). However, the risk of lymphopenia and hemoglobinopathy is also significantly increased (18). To alleviate the side effects brought by excessive preoperative treatments, it is worth predicting the histologic grade of GA. Furthermore, predicting the preoperative histologic grade can also help identify patients with a higher risk of recurrence and help select individualized and proper therapeutic strategies, which will ultimately improve the outcome.

Currently, preoperative endoscopic biopsy is used as the gold standard for the diagnosis of GA and its histologic grade (19). However, as an invasive procedure, endoscopic biopsy carries a risk of iatrogenic perforation and postendoscopic infection (20,21). Additionally, intratumor heterogeneity may inevitably produce sampling bias, and the histological results may be inconsistent with those obtained during surgery (22,23). For patients with "indefinite for neoplasm/dysplasia" lesions, the diagnostic accuracy for adenocarcinoma is even lower than 70% (24). Therefore, an auxiliary method in addition to biopsy for GA grading may be beneficial.

In clinical practice, contrast-enhanced computed tomography (CT) is used for preoperative staging of GA (19). Liu *et al*. leveraged the textures of CT images to predict gastric cancer differentiation degree, Lauren classification, and vascular invasion status (25). However, subjective selection of CT textures may cause intra- and inter-observer variability. Li *et al*. studied iodine concentration in spectral CT, which demonstrated potential in the diagnosis of gastric cancer and its histologic types (22). However, spectral CT is still not widely used. Recently, radiomics has been proposed to convert medical images into high-dimensional features, which allows high-throughput data mining and quantitative feature measurements (26,27). In addition, a number of studies have shown that radiomic feature extraction and comprehensive feature analysis are conductive to individualized management for patients (28-31). Although a previous study used radiomics signatures to predict adverse histopathological status (including WHO grade) of gastric cancer (32), an optimal prediction model combining radiomics signatures and clinical features has yet to be developed.

In this research, we aimed to associate the radiomics signature with clinical characteristics to construct and validate a radiomics nomogram to assist in predicting the histologic grade of GAs preoperatively.

Materials and methods

Patients

This study was approved by the institutional research board of Guangdong Provincial People's Hospital. The requirement for informed consent was waived because this was a retrospective study. The records and images of 738 patients with GA in Guangdong Provincial People's Hospital from January 2008 to May 2018 were collected and obtained. All these patients with GA satisfied the following inclusion criteria: 1) contrast-enhanced CT examination ≤1 month preoperatively; 2) visible tumor lesions on CT images; 3) postoperative specimen with pathologic diagnosis of histologic differentiation grade of GA; and 4) received no preoperative neoadjuvant chemotherapy or radiotherapy. A total of 146 cases were excluded from the 738 cases collected. More details can be found in *Figure 1*.

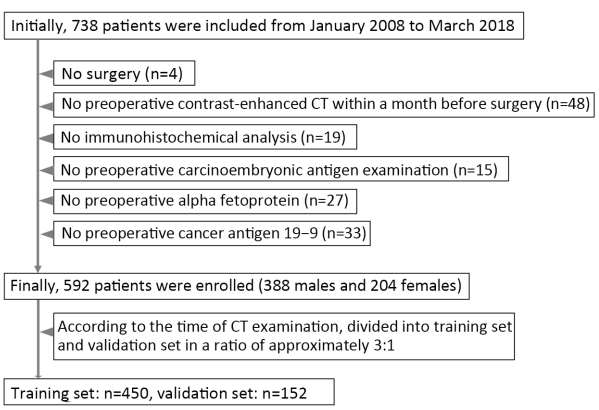

Figure 1 Flowchart of patient enrollment.

The 592 enrolled patients with GA (mean age, 58.83±12.31; range, 26–90) years were separated into training and validation sets based on the CT examination time. The training set consisted of 450 patients, and the validation set consisted of 142 patients.

We collected baseline clinicopathologic characteristics, including age, sex, clinical stage, CT-reported tumor location, preoperative carcinoembryonic antigen level (CEA, 0–5 ng/mL: normal; >5 ng/mL: abnormal), carbohydrate antigen (CA19-9, 0–27 U/mL: normal; >27 U/mL: abnormal), time of preoperative CT scan and date of surgery, preoperative and postoperative histologic grade, clinical stage, CT-reported main tumor location and T stage from the institution archives. There were no missing data for any of the clinical messages described above except for 77 missing preoperative histologic grades. The relative location of the tumor inside the stomach was also taken into consideration. According to the third edition of the Japanese classification of gastric carcinoma (33), tumors of the stomach were anatomically designated into three parts according to the main tumor location on CT: upper, middle and lower portions. The gastric stump was listed as the fourth location since it does not belong to any of the aforementioned locations. The clinical stage and CT-reported T stage were diagnosed based on the American Joint Committee on Cancer (AJCC) staging system (8th edition) (34).

Histologic grade assessment

Pathohistologic examination of each pre- and post-operative specimen was performed by two pathologists blinded to the CT findings. In concordance with the 5th edition of the WHO tumor classification of the digestive system (5) and with the consent of the two pathologists, the histologic results were divided into low- and high-grade.

CT image acquisition protocol

Before the CT scan, each patient fasted for more than 5 h and was asked to drink 600–1,000 mL of water. Then, routine non-enhanced CT was performed with multidetector row CT (MDCT) scanners, which covered the whole stomach region. Then, iodinated contrast (Ultravist 370, Bayer Schering Pharma, Berlin, Germany) was injected into the antecubital vein through an automatic power pump injector (Ulrich CT Plus 150, Ulrich Medical, Ulm, Germany) at a dose of 1.5 mL/kg and a rate of 3.5 mL/s. After 30- and 60-second delaying intervals, arterial phase and portal venous phase images were obtained, respectively. The CT scanning parameters are shown in *Supplementary Table S1*.

Radiomics feature extraction and feature analysis methodology

Since most gastric tumor lesions showed significant enhancement in the portal venous phase and could be well delineated from the adjacent tissues, CT images of this phase were obtained from the picture archiving and communication system (PACS, Carestream, Canada) for further image feature extraction. ITK-SNAP software (Version 3.6.0, http://www.itksnap.org, USA) was used for manual delineation of visible tumor contours and obtaining regions of interest (ROIs) for radiomics analysis by two radiologists with 2 and 5 years of experience in the diagnosis of gastrointestinal images (35). Intragastric air, necrosis area, enlarged lymph nodes, and perigastric adipose tissue were carefully excluded from the contours (*Figure 2*).

Then, a volume of interest (VOI) was constructed by integrating the sequences of ROIs. Before feature extraction, the CT image sequence was rescaled with one pixel size of 1 mm × 1 mm × 1.25 mm by linear interpolation. The pixels from −300 Housefield units (HU) to 700 HU were normalized to the range of [1, 100] by applying min-max normalization. After that, the radiomic features of VOIs were extracted and analyzed using the embedded algorithms provided by MATLAB R2019b (MathWorks, Natick, MA, USA). Extracted features consisted of first-order intensities, texture features, wavelet features, and shape- and size-based features.

Selection of radiomics features and construction of radiomics signature

To investigate intra- and inter-observer reproducibility, 25

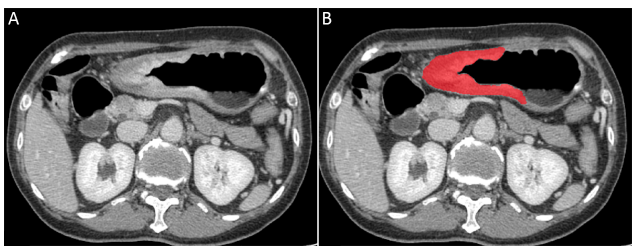

Figure 2 An example of manual segmentation in gastric adenocarcinoma. (A) A diffusely infiltrating mass with enhancement is shown on the portal venous phase CT image; (B) The manually segmented area is shown on the same axial slice.

cases were chosen randomly from the training set, and VOI delineation and radiomics feature extractions were repeated by the two radiologists. To determine the more robust features, the reproducibility and stability of the extracted features were assessed by intra- and inter-class correlation coefficients (ICCs), which were calculated based on feature extractions by reader 1 twice and once by each of the two readers, respectively. Only stable features with ICC>0.90 were reserved (36).

For data standardization, features of the training and validation sets were first normalized by the mean ($\bar{X}$) and standard deviation (SD) of the training set with z-score according to the following formula:

$$X' = \left(X - \bar{X}\right) / SD.$$

To reduce the feature dimension and to filter out redundant features, the Wilcoxon rank-sum test was introduced to further determine the features with a statistically significant difference (P<0.05) in two labels from the preselected features. The least absolute shrinkage and selection operator regression (LASSO) algorithm was utilized for final dimensionality reduction. Ten-fold cross-validation was used to select the tuning parameter (λ) by using the minimum criteria and 1 standard error of the minimum criteria (the 1-SE criteria). To lower the risk of overfitting, the log (λ) corresponding to 1-SE was chosen, where there are 12 nonzero coefficients. The details are provided in *Figure 3*. The features with the most significance and the best reproducibility were ultimately preserved. After that, the coefficients of each feature were calculated by a generalized linear model. The radiomics score, i.e., the Rad-score, of every single patient was calculated by a weighted linear combination of the features and their corresponding coefficients.

Assessment of radiomics signature predictive performance

The discriminative power of the radiomics signature was tested by the receiver operating characteristic (ROC) curve. The maximum positive likelihood ratio (true positive value/false positive value) was used to determine the optimal cutoff value. Note that the cutoff value of the validation set was directly drawn from the training set to guarantee independence. The specificity, sensitivity and accuracy were also computed using the same cutoff value. The area under the receiver operating characteristic curve (AUC) was also introduced to evaluate the effectiveness of the predictive model in both the training and validation sets.

Radiomics nomogram construction

Multivariable logistic regression analysis was performed to establish a prediction model by combining the radiomics signature and independent clinicopathologic predictors

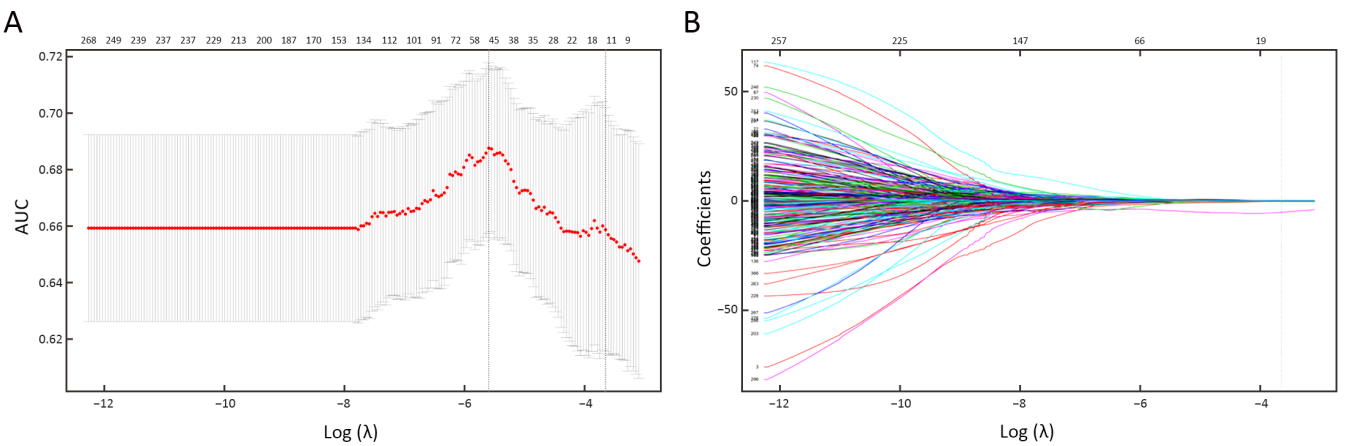

Figure 3 Feature selection with LASSO binary logistic regression model. (A) Tuning parameter (λ) selection in the LASSO model using 10-fold cross-validation. AUC was plotted *vs*. log (λ). Using the minimum criteria and the 1 standard error of the minimum criteria (the 1-SE criteria), dotted vertical lines were drawn at the best value. The 1-SE criteria were chosen according to 10-fold cross-validation, whereas 12 radiomics features were chosen; (B) LASSO coefficient profiles of features. A coefficient profile plot was plotted *vs*. log (λ). As λ becomes larger, the coefficients of more features shrunk to 0. Each colored line represents the coefficient of each feature. The vertical grey line was drawn at the selected λ, where 12 features had nonzero coefficients. LASSO, least absolute shrinkage and selection operator; AUC, area under the receiver operating characteristic curve.

with P values less than 0.05 in the univariable analysis. We visualized the model as a radiomics nomogram in the training set based on multivariable logistic analysis to promote the clinical application value of the prediction model.

Assessment of radiomics nomogram predictive performance

The ROC curve was applied in the assessment of the discriminative performance of the radiomics nomogram. DeLong's test was executed to calculate the statistical significance in comparing differences in AUCs between the radiomics nomogram and the clinical model and between the radiomics nomogram and biopsy results. The radiomics nomogram was assessed by a calibration curve.

Statistical analysis

Statistical analysis was performed using IBM SPSS Statistics (Version 26.0; IBM Corp., New York, USA) and R software (Version 3.5.1; R Foundation for Statistical Computing, Vienna, Austria). Student's *t* test and Pearson Chi-square test were used to compare continuous and categorical data, respectively. All P values were two sided, and P<0.05 was considered statistically significant.

Results

Clinical characteristics

In the total 592 cases included, 515 accepted preoperative biopsies, among which 97 with preoperative diagnosis of low-grade GA and 346 patients with preoperative diagnosis of high-grade GA had identical postoperative results as the preoperative ones. Forty of the patients who were preoperatively diagnosed with low-grade GA were postoperatively diagnosed with high-grade GA; among them, 28 patients' radiomic results were consistent with their postoperative results. Thirty two of the patients who were preoperatively diagnosed with high-grade GA had postoperative low-grade results; among them, 23 patients' radiomic results were consistent with their postoperative low-grade results. The training set consisted of 300 males and 150 females, with average age of 58.54±12.29 (range: 26–90) years, and the validation set consisted of 88 males and 54 females, with average age of 59.77±12.38 (range: 30–87) years. No statistically significant difference was found in age or sex between the training and validation sets (P=0.296; P=0.305, respectively).

Table 1 demonstrates the clinical characteristics of

Table 1 Characteristics of patients in training and validation sets

Characteristics	Training set [n (%)] (N=450)			Validation set [n (%)] (N=142)		
	Low grade	High grade	P*	Low grade	High grade	P*
Age ($\bar{x}\pm s$) (year)	61.55±9.91	57.59±12.81	0.001	64.04±10.99	57.66±12.54	0.004
Gender			0.003			<0.001
Male	84 (78.5)	216 (63.0)		40 (85.1)	48 (50.5)	
Female	23 (21.5)	127 (37.0)		7 (14.9)	47 (49.5)	
CEA level			0.029			0.598
Normal	81 (75.7)	291 (84.8)		39 (83.0)	82 (86.3)	
Abnormal	26 (24.3)	52 (15.2)		8 (17.0)	13 (13.7)	
CA19-9 level			0.084			0.980
Normal	77 (72.0)	274 (79.9)		40 (85.1)	81 (85.3)	
Abnormal	30 (28.0)	69 (20.1)		7 (14.9)	14 (14.7)	
Tumor location**			<0.001			<0.001
Upper-third	47 (43.9)	57 (16.6)		23 (48.9)	8 (8.4)	
Middle-third	16 (15.0)	106 (30.9)		12 (25.5)	47 (49.5)	
Lower-third	43 (40.2)	178 (51.9)		11 (23.4)	40 (42.1)	
Gastric stump	1 (0.9)	2 (0.6)		1 (2.1)	0 (0)	
Rad-score (95% CI)	0.283 (0.222–0.363)	0.215 (0.139–0.282)	<0.001	0.302 (0.211–0.335)	0.189 (0.139–0.271)	<0.001

CEA, carcinoembryonic antigen; CA 19-9, carbohydrate antigen 19-9; 95% CI, 95% confidence interval; *, Continuous variables were compared using student *t* test while categorical variables were compared using Chi-square test; **, Tumors of the stomach were categorized into four parts based on the main tumor location reported by CT.

patients included in the study. Age, sex and tumor location exhibited significant differences between patients with low- and high-grade GAs in both the training and validation sets (P=0.001 and P=0.004; P=0.003 and P<0.001; P<0.001 and P<0.001). In contrast, CEA and CA19-9 levels showed no significant difference between them in either the training or validation sets (P>0.05).

Radiomics features reproducibility

For each patient, the VOI was extended into a total of 16,384 three-dimensional radiomics features, of which 9,449 features were strongly reproducible (ICC>0.90). For further selection, the Wilcoxon rank-sum test was conducted to filter the features with statistically significant differences between GA of different grades and drew 427 filtered features.

Radiomics features selection and signature construction

The LASSO logistic regression model was used to select the final 12 features with relatively high predictive outcome from the 427 robust features in the training set (*Figure 3A,B*). The radiomics score (Rad-score) of each case with GA was calculated by a weighted linear combination of these twelve features and their corresponding coefficients.

Radiomics signature predictive performance

For low- and high-grade GA patients, the median Rad-scores were 0.283 and 0.215 in the training set and 0.302 and 0.189 in the validation set, respectively. Regardless of the training set or the validation set, the median Rad-scores in the low-grade group were higher than those in the high-grade group (P<0.001 for both). The ROC curves shown in *Figure 4* yield AUCs of 0.705 [95% confidence interval (95% CI): 0.650–0.760] for the training set and 0.720 (95% CI: 0.630–0.810) for the validation set, demonstrating the discriminative power of the radiomics signature. The statistical results, including sensitivity, specificity, positive predictive value (PPV), negative predictive value (NPV) and accuracy, are demonstrated in *Table 2*.

Radiomics nomogram construction

In the univariate analysis, sex, age, radiomics score, CEA

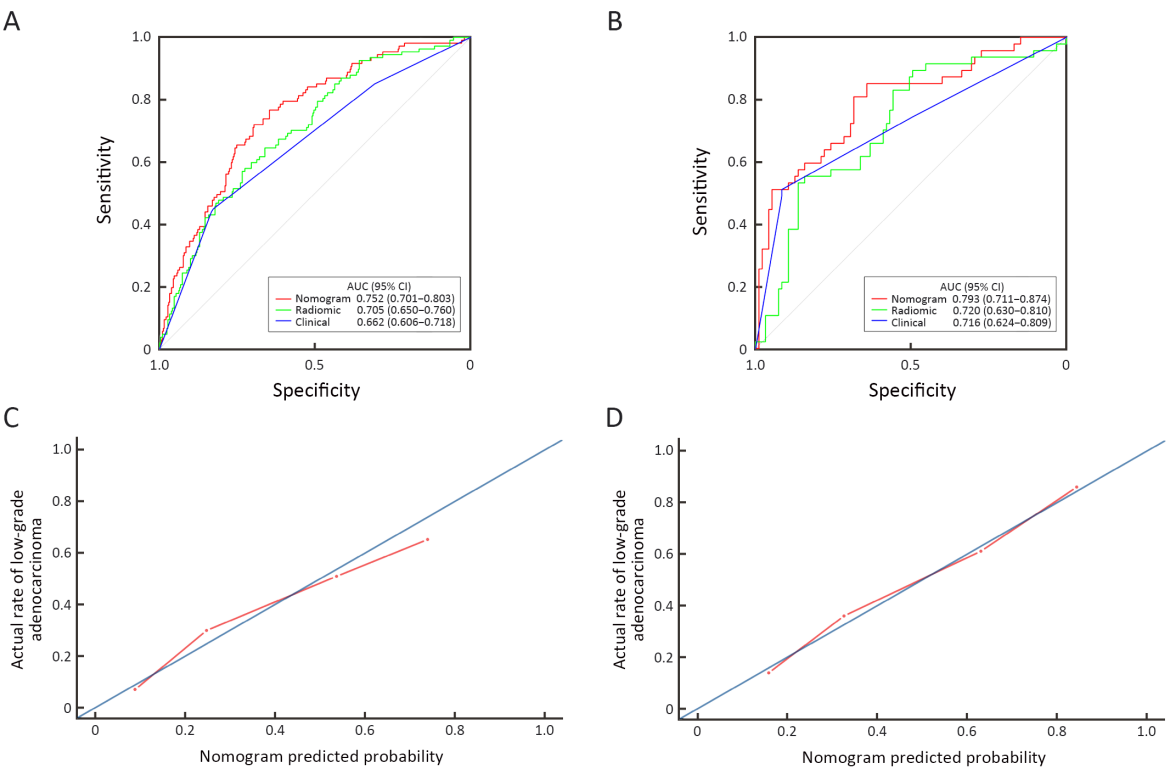

Figure 4 Receiver operating characteristic (ROC) curves of radiomics nomogram, radiomics signature and tumor location alone in training set (A) and validation set (B) respectively. Calibration curves of radiomics nomogram in the training set (C) and the validation set (D). AUC, area under the receiver operating characteristic curve; 95% CI, 95% confidence interval.

Table 2 Predictive performance of radiomics nomogram, clinical characteristics and radiomics signature in training and validation sets

Predictive performance	AUC (95% CI)	Sensitivity	Specificity	PPV	NPV	Accuracy
Training-nomogram	0.752 (0.701–0.803)	0.697	0.720	0.888	0.425	0.702
Validation-nomogram	0.793 (0.711–0.874)	0.947	0.511	0.796	0.828	0.803
Training-clinic	0.662 (0.606–0.718)	0.828	0.449	0.828	0.449	0.738
Validation-clinic	0.716 (0.624–0.809)	0.916	0.511	0.791	0.750	0.782
Training-radiomic	0.705 (0.650–0.760)	0.659	0.645	0.856	0.371	0.656
Validation-radiomic	0.720 (0.630–0.810)	0.842	0.553	0.792	0.634	0.746

AUC, area under the receiver operating characteristic curve; 95% CI, 95% confidence interval; PPV, positive predictive value; NPV, negative predictive value.

level and tumor location were associated with the histologic grade of GA. Multivariable logistic regression analysis identified the radiomics score and tumor location as independent predictors (*Table 3*). The tumor location was integrated into the nomogram with the radiomics signature (*Figure 5*).

Radiomics nomogram predictive performance

Figure 4 demonstrates the ROC curves of the radiomics nomogram, radiomics signature and tumor location alone. The radiomics nomogram demonstrated relatively good discriminative power for histologic grade prediction among the three indicators, with improvements in the AUC from 0.662 for the clinical model to 0.752 (P<0.05, DeLong's test) in the training set and from 0.716 for the clinical model to 0.793 (P=0.03, DeLong's test) in the validation set. In our datasets, biopsy outperformed the nomogram, with AUCs of 0.824 in the training set (P<0.05, DeLong's test) and 0.825 in the validation set (P<0.05, DeLong's test). The calibration curve of the radiomics nomogram shown in *Figure 4* depicted good agreement between the observed outcome and the prediction.

Discussion

In this study, a radiomics nomogram that preoperatively predicts the histologic grade of GA based on tumor location and radiomics signatures extracted from CT images was developed and validated. It demonstrated AUCs of 0.752 and 0.793 in the training and validation sets, respectively.

In practice, surgeons conventionally use endoscopic biopsy for the diagnosis of GA and its histologic grade. However, the risks of gastric perforation, bleeding, abdominal pain, postendoscopic infection, and an overall discordance rate of 21.5% between pathohistologic results of endoscopic biopsy and postoperative specimens in mucosal GA indicates a rather limited value of endoscopic biopsy (19-21,37). The comparison between the preoperative and postoperative pathohistologic results of

Table 3 Univariable and multivariable analysis of risk factors

Risk factors	Univariable analysis			Multivariable analysis		
	OR	95% CI	P	OR	95% CI	P
Gender	2.147	1.289–3.578	0.003	1.364	0.781–2.383	0.276
Age	0.973	0.955–0.991	0.004	0.980	0.959–1.001	0.066
Radiomics score	0	0–0.010	<0.001	0.003	0–0.028	<0.001
CEA level	0.557	0.327–0.947	0.031	0.718	0.401–1.284	0.264
CA19-9 level	0.646	0.393–1.063	0.086			
Location						
Upper-third	Ref			Ref		
Middle-third	5.463	2.845–10.488	<0.001	3.380	1.682–6.791	<0.001
Lower-third	3.413	2.050–5.684	<0.001	2.526	0.211–0.615	<0.001
Gastric stump	1.649	0.145–18.757	0.687	1.619	0.033–8.194	0.813

CEA, carcinoembryonic antigen; CA 19-9, carbohydrate antigen 19-9; OR, odds ratio; 95% CI, 95% confidence interval.

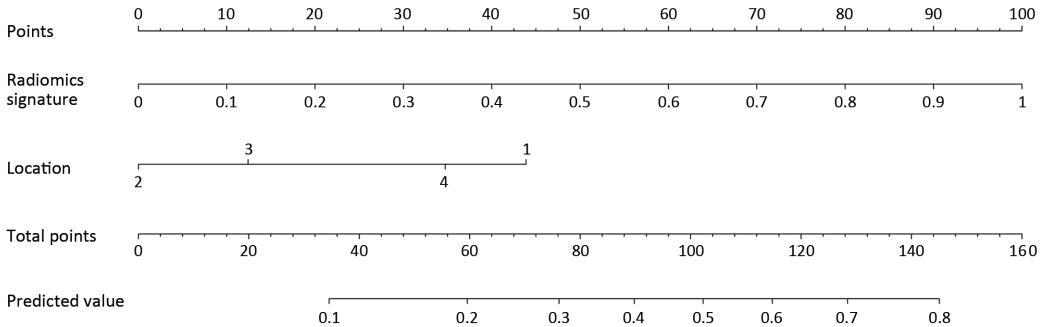

Figure 5 Developed radiomics nomogram. The radiomics nomogram was developed in the training set with radiomics signature and tumor location incorporated. Location, tumor location of the stomach (1, upper-third; 2, middle-third; 3, lower-third; 4, gastric stump).

our study also exhibited a difference of 13.98%, which further verifies that the existence of intra-tumor heterogeneity could lead to a substantial discordance rate while affecting clinical decisions. Thus, researchers are now investigating auxiliary noninvasive approaches to precisely predict the histologic grade of GA preoperatively. A previous study analyzed CT texture to predict patho-histological characteristics, including the differentiation degree of gastric cancer, with a sensitivity of 78.7% and a specificity of 83.3% (25). However, CT texture is subjectively assessed and may lead to intra- and inter-observer variability. Therefore, we controlled this variability in our study by constructing a radiomics signature with more reproducible radiomics features (ICC>0.90). Lin *et al*. explored and discovered the potential diagnostic significance of preoperative CEA/CA19-9 levels (38), so we included these tumor markers in our study, in addition to other clinical and semantic imaging data, including age, sex and CT-reported tumor location, which were analyzed by univariable analysis. Then, a radiomics nomogram was modeled by combining the radiomics features with independent predictive factors drawn by multivariable analysis. In 2018, a published study showed that normalized arterial phase iodine concentration in spectral CT demonstrated a high efficiency in diagnosing poorly differentiated GA (22). Currently, spectral CT is not widely used in daily clinical practice. Li *et al*. applied machine learning-based computational models to predict adverse histopathological status, including WHO grade, of gastric cancer, with AUCs of 0.65 and 0.63 in the training and validation sets, respectively (32), while the AUCs of the radiomics nomogram developed in our study were higher (0.752 in the training set and 0.793 in the validation set). Although biopsy outperformed the radiomics model in our study, as a noninvasive method, radiomics still has the potential to aid in diagnosis when the patient cannot tolerate an endoscopic examination due to coagulation disorders or critically ill status or refuses to undergo endoscopy. Since contrast-enhanced CT is routinely performed for the staging and management of GA, CT-based radiomics nomograms may be more applicable and more popular in clinical practice. The nomogram may facilitate preoperative identification of patients with a higher risk of recurrence, worse clinicopathological features and poorer prognosis.

There are some limitations in this study. The radiomics features used in the study were extracted only from the portal venous phase CT images because the differentiation between the tumor and the adjacent normal gastric tissues was maximal in this phase. Nonenhanced scans, arterial phase, and venous phase images with extracted radiomics features should be investigated in further studies. Because of our retrospective collection of cases, the quality of CT images acquired by different CT machines may be unstable. Prospective studies are expected to avoid confounding factors and to assure discriminative power in GA histologic grades of radiomics signatures.

Conclusions

A radiomics nomogram in discriminating low-grade GA from high-grade GA before treatment was developed and validated. As a quantitative and noninvasive approach, the radiomics nomogram may play a part in facilitating personalized management and improving outcomes of patients with GA.

Acknowledgements

This study was supported by the National Key Research and Development Program of China (No. 2017YFC

1309100), the National Science Fund for Distinguished Young Scholars (No. 81925023), and the National Natural Science Foundation of China (No. 82071892, 81771912, 81901910).

Footnote

Conflicts of Interest: The authors have no conflicts of interest to declare.

References

1. Wu JY, Lee YC, Graham DY. The eradication of Helicobacter pylori to prevent gastric cancer: a critical appraisal. Expert Rev Gastroenterol Hepatol 2019; 13:17-24.
2. Bray F, Ferlay J, Soerjomataram I, et al. Global cancer statistics 2018: GLOBOCAN estimates of incidence and mortality worldwide for 36 cancers in 185 countries. CA Cancer J Clin 2018;68:394-424.
3. Stewart BW, Wild CP. World Cancer Report 2014. IARC: Non-Serial Publications. Available online: https://publications.iarc.fr/Non-Series-Publications/World-Cancer-Reports/World-Cancer-Report-2014
4. Dicken BJ, Bigam DL, Cass C, et al. Gastric adenocarcinoma: Review and considerations for future directions. Ann Surg 2005;241:27-39.
5. Bosman FT, Carneiro F, Hruban RH, et al. WHO classification of tumours of the digestive system. IARC: Lyon, 2010. Available online: https://publications.iarc.fr/Book-And-Report-Series/Who-Classification-Of-Tumours/WHO-Classification-Of-Tumours-Of-The-Digestive-System-2010
6. Nagtegaal ID, Odze RD, Klimstra D, et al. The 2019 WHO classification of tumours of the digestive system. Histopathology 2020;76:182-8.
7. Feng F, Liu J, Wang F, et al. Prognostic value of differentiation status in gastric cancer. BMC Cancer 2018;18:865.
8. Piessen G, Messager M, Leteurtre E, et al. Signet ring cell histology is an independent predictor of poor prognosis in gastric adenocarcinoma regardless of tumoral clinical presentation. Ann Surg 2009; 250:878-87.
9. Cai L, Li Y, Yang XW, et al. Prognostic significance of mucinous component in gastric adenocarcinoma after radical D2 gastrectomy. Onco Targets Ther 2018;11:967-73.
10. Adachi Y, Yasuda K, Inomata M, et al. Pathology and prognosis of gastric carcinoma: well versus poorly differentiated type. Cancer 2000;89:1418-24.
11. Kanesaka T, Nagahama T, Uedo N, et al. Clinical predictors of histologic type of gastric cancer. Gastrointest Endosc 2018;87:1014-22.
12. Marrelli D, Morgagni P, de Manzoni G, et al. Prognostic value of the 7th AJCC/UICC TNM classification of noncardia gastric cancer: Analysis of a large series from specialized western centers. Ann Surg 2012;255:486-91.
13. Deng J, Liang H, Sun D, et al. Suitability of 7th UICC N stage for predicting the overall survival of gastric cancer patients after curative resection in China. Ann Surg Oncol 2010;17:1259-66.
14. Lee HH, Song KY, Park CH, et al. Undifferentiated-type gastric adenocarcinoma: prognostic impact of three histological types. World J Surg Oncol 2012;10:254.
15. Shin CH, Lee WY, Hong SW, et al. Characteristics of gastric cancer recurrence five or more years after curative gastrectomy. Chin J Cancer Res 2016;28:503-10.
16. Al-Batran SE, Homann N, Pauligk C, et al. Effect of neoadjuvant chemotherapy followed by surgical resection on survival in patients with limited metastatic gastric or gastroesophageal junction cancer: The AIO-FLOT3 trial. JAMA Oncol 2017;3:1237-44.
17. Das M. Neoadjuvant chemotherapy: survival benefit in gastric cancer. Lancet Oncol 2017;18:e307.
18. Miao ZF, Liu XY, Wang ZN, et al. Effect of neoadjuvant chemotherapy in patients with gastric cancer: a PRISMA-compliant systematic review and meta-analysis. BMC Cancer 2018;18:118.
19. Ajani JA, D'Amico TA, Almhanna K. Gastric cancer, version 3.2016, NCCN Practice Guidelines in Oncology. J Natl Compr Canc Netw 2016;14:1286-312.
20. Al Ghossaini N, Lucidarme D, Bulois P. Endoscopic treatment of iatrogenic gastrointestinal perforations: an overview. Dig Liver Dis 2014;46:195-203.
21. Wang P, Xu T, Ngamruengphong S, et al. Rates of infection after colonoscopy and osophagogastro-duodenoscopy in ambulatory surgery centres in the USA. Gut 2018;67:1626-36.
22. Li R, Li J, Wang X, et al. Detection of gastric cancer and its histological type based on iodine concentration

in spectral CT. Cancer Imaging 2018;18:42.
23. Gerlinger M, Rowan AJ, Horswell S, et al. Intratumor heterogeneity and branched evolution revealed by multiregion sequencing. N Engl J Med 2012;366:883-92.
24. Kwon MJ, Kang HS, Kim HT, et al. Treatment for gastric "indefinite for neoplasm/dysplasia" lesions based on predictive factors. World J Gastroenterol 2019;25:469-84.
25. Liu S, Liu S, Ji C, et al. Application of CT texture analysis in predicting histopathological characteristics of gastric cancers. Eur Radiol 2017;27:4951-9.
26. Gillies RJ, Kinahan PE, Hricak H. Radiomics: Images are more than pictures, they are data. Radiology 2016;278:563-77.
27. Lambin P, Leijenaar RTH, Deist TM, et al. Radiomics: The bridge between medical imaging and personalized medicine. Nat Rev Clin Oncol 2017; 14:749-62.
28. Beig N, Khorrami M, Alilou M, et al. Perinodular and intranodular radiomic features on lung CT images distinguish adenocarcinomas from granulomas. Radiology 2019;290:783-92.
29. Huang Y, Liu Z, He L, et al. Radiomics signature: a potential biomarker for the prediction of disease-free survival in early-stage (I or II) non-small cell lung cancer. Radiology 2016;281:947-57.
30. Huang YQ, Liang CH, He L, et al. Development and validation of a radiomics nomogram for preoperative prediction of lymph node metastasis in colorectal cancer. J Clin Oncol 2016;34:2157-64.
31. Huang X, Cheng Z, Huang Y, et al. CT-based radiomics signature to discriminate high-grade from low-grade colorectal adenocarcinoma. Acad Radiol 2018;25:1285-97.
32. Li Q, Qi L, Feng QX, et al. Machine learning-based computational models derived from large-scale radiographic-radiomic images can help predict adverse histopathological status of gastric cancer. Clin Transl Gastroenterol 2019;10:e00079.
33. Japanese Gastric Cancer Association. Japanese classification of gastric carcinoma: 3rd English edition. Gastric Cancer 2011;14:101-12.
34. Amin MB, Edge S, Greene F, et al. AJCC Cancer Staging Manual. Eighth edition. Springer International Publishing; 2017. Available online: https://www.springer.com/gp/book/9783319406176
35. Yushkevich PA, Piven J, Hazlett HC, et al. User-guided 3D active contour segmentation of anatomical structures: significantly improved efficiency and reliability. Neuroimage 2006;31:1116-28.
36. Gstoettner M, Sekyra K, Walochnik N, et al. Inter- and intraobserver reliability assessment of the Cobb angle: manual versus digital measurement tools. Eur Spine J 2007;16:1587-92.
37. Lee IS, Park YS, Lee JH, et al. Pathologic discordance of differentiation between endoscopic biopsy and postoperative specimen in mucosal gastric adenocarcinomas. Ann Surg Oncol 2013;20:4231-7.
38. Lin JX, Wang W, Lin JP, et al. Preoperative tumor markers independently predict survival in stage III gastric cancer patients: should we include tumor markers in AJCC staging? Ann Surg Oncol 2018; 25:2703-12.

Cite this article as: Huang J, Yao H, Li Y, Dong M, Han C, He L, Huang X, Xia T, Yi Z, Wang H, Zhang Y, He J, Liang C, Liu Z. Development and validation of a CT-based radiomics nomogram for preoperative prediction of tumor histologic grade in gastric adenocarcinoma. Chin J Cancer Res 2021;33(1):69-78. doi: 10.21147/j.issn.1000-9604.2021.01.08

Table S1 CT scanning parameters for patients

Scanner	kV (mAs)*	Rotation time (s)	Detector collimation (mm)	Field of view (mm^2)	Matrix	Reconstruction section thickness (mm)	Acquisition time (s)	
							Arterial phase	Portal venous phase
256-slice Brilliance iCT (Philips Healthcare, Cleveland, Ohio, USA)	120	0.5	128×0.625	360×360	512×512	1.00	30	60
64-slice LightSpeed VCT (GE Medical systems, Milwaukee, WI, USA)	120	0.4	64×0.625	360×360	512×512	1.25	30	60

*, The tube current is automatically selected based on the attenuation of each scanning object and ranges from 100 to 300 mAs.